Chapter 4

PROTEOMIC RESPONSE OF AN ANTIBIOTIC-TOLERANT BIOFILM SUBPOPULATION TO CIPROFLOXACIN

4.1 Abstract

Chronic biofilm infections are of particular concern due to their increased tolerance to antibiotics. The study of biofilms *in vitro* is complicated by phenotypic heterogeneity which results in biofilm subpopulations with differential responses to antibiotics. To better understand the physiology of tolerance, we adapt the bioorthogonal noncanonical amino acid tagging (BONCAT) method for selective proteomics to target a *Pseudomonas aeruginosa* biofilm subpopulation. We target protein labeling to interior regions of biofilm microcolonies through the use of the endogenous *rpoS* promoter and show successful enrichment and identification of newly synthesized proteins from this region. We perform a pulse-labeling experiment to measure the dynamic proteomic response of this tolerant subpopulation to supra-MIC treatment with the fluoroquinolone ciprofloxacin. We find upregulation of proteins involved in flagellar motility and purine synthesis as well as a substantial rearrangement of enzymes involved in central carbon metabolism.

4.2 Introduction

Bacteria living as surface-associated biofilms exhibit increased tolerance to a wide-variety of stresses as compared to their planktonic counterparts [1]. Of clinical importance is the increased tolerance to antibiotics that prohibits the elimination of chronic biofilm infections. This phenotypic tolerance is distinct from genotypic resistance, though the evolution of resistance can be exacerbated by the persistence of cells that survive treatment [2]. The opportunistic pathogen *Pseudomonas aeruginosa* serves as a model system for both biofilm physiology as well as antibiotic tolerant infection. *P. aeruginosa* is a primary contributor to chronic infections of the cystic fibrosis lung, where it forms biofilms that are recalcitrant to the host immune system and treatment by antibiotics. Tolerance of these biofilm infections has been well characterized within the host [3], and through *in vitro* studies of biofilms [4].

Moreover, detailed analyses of bacterial biofilms grown *in vitro* have revealed the role of spatial heterogeneity in their response to antibiotics; specific subpopulations survive treatment while others do not [1, 5]. Similar to their differential effects on fast growing vs. slow growing planktonic cells, drug classes like fluoroquinolones (DNA replication) [6], aminoglycosides (translation) [7], and β-lactams (peptidoglycan synthesis) [8] that target active processes kill growing cells within biofilm regions that have greater access to exogenous nutrients. Conversely, polymyxins and detergents that disrupt cellular membranes preferentially kill dormant cells in the interior of biofilm microstructures [6]. Explanations for the spatial segregation of antibiotic responses include the reduced penetration of small molecule antibiotics, lowered metabolic rates, and altered physiology [1, 5].

Measurements of mRNA or protein abundances have offered unbiased views of physiological responses to antibiotics [9–11] but a variety of challenges limit the investigation of tolerant biofilm subpopulations. Because only a subpopulation of cells exhibit tolerance, any analysis ought to distinguish tolerant cells from those that do not survive treatment. Laser capture micro dissection has been used to isolate biofilm cells from spatially distinct regions of biofilms and quantitative PCR (qPCR) and DNA microarray analyses have been used to quantify differences in mRNA transcript abundances [12, 13]. This approach has not been applied to understand the heterogeneous response to antibiotics. Proteomic measurements have been widely used to better understand biofilm physiology [14], but selective approaches have been limited. Physical separation is challenging due to the small length scales

involved, and manual selection of subpopulations of interest can introduce human error into the analysis. In addition, an open question is what differences exist, if any, between the instantaneous response to antibiotic stress and the long-term phenotypic adaptation.

An important recent technological advance is the application of pulsed stable isotope labeling with amino acids (pSILAC) to quantify changes in protein expression following adaptation of biofilm cells to challenge with the clinical polymixin antibiotic colistin [15]. By pulsed addition of an amino acid isotoplog, pSILAC provides a means to distinguish——by mass——proteins synthesized before and after the pulse [16] . Chua, *et al.* treated biofilms with colistin for 8 h thereby allowing non-tolerant cells to die, and then labeled new protein synthesis with an extended (48 h) amino acid isotpolog pulse, ensuring that labeled proteins were made by the tolerant subpopulation of interest. This approach revealed an importance for type IV-mediated motility in the resistance to colistin.

To address the challenges of phenotypic heterogeneity and dynamic responses, we employed the bioorthogonal noncanonical amino acid tagging (BONCAT) method for selective proteomics [17, 18]. BONCAT relies on the cellular incorporation of a non-canonical amino acid (ncAA) that bears a bioorthogonal chemical handle. Following incorporation, labeled proteins can be reacted to an affinity tag and enriched from the pool of unlabeled proteins. Enriched proteins can be identified and quantified via liquid chromatography-tandem mass spectrometry (LC-MS/MS). Like pSILAC, BONCAT allows for temporal selectivity; proteins synthesized during the ncAA pulse are chemically distinct from pre-existing proteins. However, a key advantage of the enrichment-based proteomics method is that proteins of interest can be physical separated from the rest of the proteome. MS-based protein identification is sensitive to the complexity of the sample, such that proteins of low abundance often go unidentified, so reducing sample complexity can aid in the identification of proteins of interest. We and others have shown the exquisite temporal sensitivity of BONCAT-based enrichment in the context of dynamic proteome changes [19, 20]. In bacteria, ncAA pulse times of a few minutes have been used to quantify dynamic processes in *Vibrio harveyi* [21, 22], *Escherichia coli* [23], and *Bacillus subtilis* [24].

BONCAT labeling can be targeted with greater precision to cell types of interest through the use of a ncAA that is not incorporated by endogenous translational machinery. However, cells expressing a mutant aminoacyl-tRNA synthetase (mRS)

that has been engineered to charge this ncAA will be labeled. Such noncanonical synthetases have been developed for the methionine surrogates azidonorleucine [25] and 2-aminooctynoic acid [26] and the phenylalanine surrogate azidophenylalanine [27]. By restricting expression of the mRS to cell types of interest, protein labeling can be targeted to a subpopulation of cells within a complex heterogeneous system. In bacteria, cell targeting can be accomplished by genetically restricting the mRS gene to a species of interest (e.g., bacteria in the presence of host cells [26, 28]) or by placing mRS expression under endogenous control of a cell-state specific promoter (e.g., reactive oxygen stress in *E. coli* [29]).

Here, we describe an adaptation of the BONCAT method for cell- and time-resolved analysis of protein synthesis in heterogeneous bacterial biofilms. We direct cell selective labeling of protein synthesis with azidonorleucine (Anl) through controlled expression of its corresponding mutant methionyl-tRNA synthetase (NLL-MetRS). We use this approach to analyze the time course of proteomic responses to ciprofloxacin stress by a biofilm subpopulation of *P. aeruginosa*.

4.3 Results

The *rpoS* Promoter Enables Cell-state Selective Labeling in Planktonic Cells

To selectively target antibiotic-tolerant biofilm cells, we aimed to restrict labeling by placing NLL-MetRS expression under control of an endogenous, cell-state selective promoter. Because regions more tolerant to many antibiotics contain cells with decreased metabolic rates, we reasoned that the use of a promoter whose activity increases during planktonic stationary phase, when metabolic rates are similarly decreased, might provide the desired selectivity. Cellular levels of the alternative sigma factor σ^{54} are upregulated in response to a variety of stresses. In *P. aeruginosa* and other bacteria σ^{54}——encoded by the gene *rpoS*——is upregulated during the transition from exponential to stationary phase during planktonic growth [30]. We hypothesized that the *rpoS* promoter would enable selective protein labeling.

We first evaluated the activity of the *rpoS* promoter in planktonic cells. We cloned the 1 kb region upstream of the endogenous *rpoS* gene 5' to *gfp* and transposed this expression cassette to the *Tn7* locus in *P. aeruginosa* PA14 (P_{rpoS}*:gfp*) (Figure 4.1A). Fluorescent imaging of P_{rpoS}*:gfp* throughout growth from early exponential phase (150 min following dilution) to late stationary phase (overnight) revealed the expected increase of promoter activity at higher cell densities (Figure 4.1B). Additionally, we noticed cellular heterogeneities in the expression of GFP. At the early

time point, only a small subpopulation of cells was GFP positive. The GFP-positive fraction increased in the early exponential time point and after overnight growth essentially all cells were expressing GFP. In contrast, wild-type cells exhibited no fluorescence (Figure 4.S1A) and when GFP expression was placed under control of the strong, constitutive *trc* promoter [31], all cells were GFP-positive at all time points (Figure 4.S1B).

Encouraged by these results, we generated a strain in which expression of an NLL-MetRS:mCherry translational fusion was controlled by the *rpoS* promoter, P_{rpoS}*:nll-mc* (Figure 4.1A). We appended this protein with an N-terminal 6x histidine tag to allow for Western blot detection of protein expression. We grew this strain from early exponential phase to stationary phase and treated samples of the culture with Anl for 15 min at three points throughout growth (Figure 4.1C). As a positive control, we treated PA14 containing a plasmid expressing NLL-MetRS under control of the P_{ara} arabinose-inducible promoter with arabinose and Anl during exponential phase. Consistent with our GFP measurements, Western blotting showed growth phase-dependent expression of NLL-MetRS when controlled by the *rpoS* promoter (Figure 4.1D). To detect Anl incorporation, we reacted cell lysates with alkyne-tetramethylrhodamine (TAMRA) under copper catalyzed click conditions, separated proteins via SDS-PAGE, and imaged fluorescence. In early exponential phase, when NLL-MetRS was not present, labeling was not detected. Labeling was strongest in late exponential phase, when NLL-MetRS expression was moderate, and low but detectable in stationary phase. For all conditions Coomassie staining was used to verify equal protein loading. The rate of Anl incorporation is dependent on both the presence of the NLL-MetRS and the overall rate protein synthesis, so we interpret the observed lower levels of Anl labeling in stationary phase as a reflection of the decreased rates of protein synthesis in this state.

Spatially Targeted Proteomics in Biofilms

To test for subpopulation targeting in biofilms, we cultured biofilms on glass coverslips under constant media flow in flow cells. Four day old biofilms were treated with Anl for 1.5 h and Anl incorporation was visualized by treating fixed biofilms with dibenzocyclooctyne (DBCO)-TAMRA. The strained-alkyne present in DBCO allows for copper-free azide-alkyne cycloaddition and removes the requirement for simultaneous diffusion of the ligand, copper catalyst, and reductant throughout biofilm microcolonies. A strain expressing NLL-MetRS constitutively (P_{trc}*:nll-mc*) was labeled throughout biofilm structures, while P_{rpoS}*:nll-mc* exhibited labeling

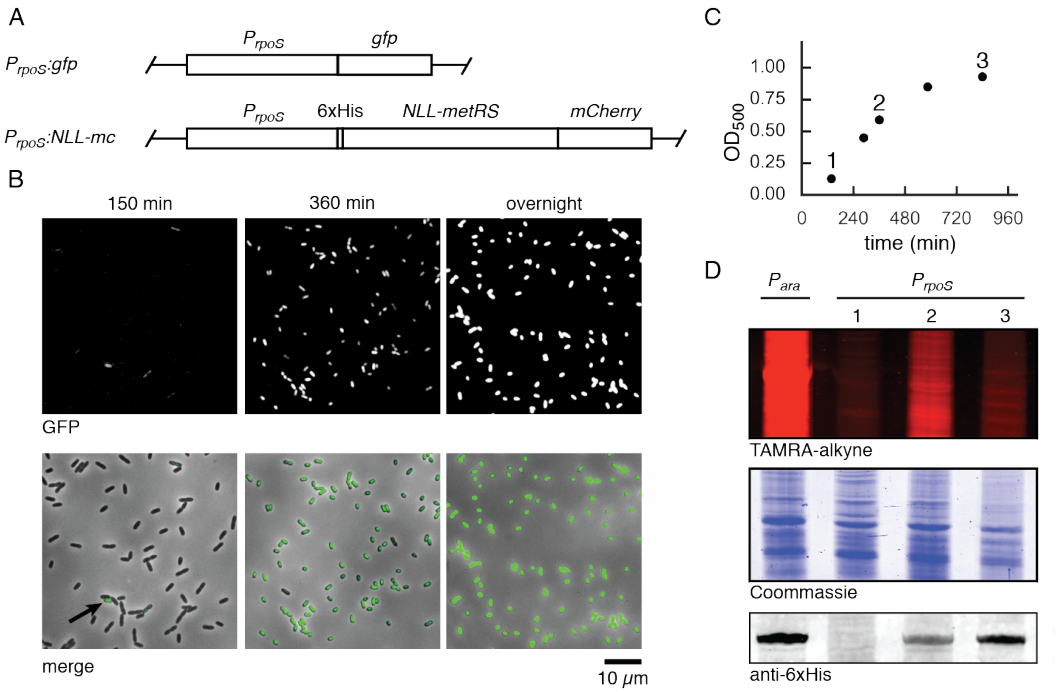

Figure 4.1: **Cell state-selective labeling using the *rpoS* promoter.** (A) *P. aeruginosa* was engineered to express GFP or an NLL-MetRS:mCherry translational fusion under control of the endogenous *rpoS* promoter. Expression cassettes were transposed to the neutral *Tn7* neutral chromosomal locus. (B) Representative images of GFP fluorescence of the P_{rpoS}*:gfp* strain throughout growth. GFP fluorescence (top) and GFP-bright field merge (bottom). Arrow indicates a GFP-positive cell in the early time point. (C) Growth curve of P_{rpoS}*:nll-mc*. At each labeled time point, an aliquot was removed and incubated with 1 mM Anl for 15 min. (D) Lysates were reacted with alkyne-TAMRA and separated via SDS-PAGE to visualize Anl incorporation. Coomassie staining of the same gel indicates equal protein loading. Lysates were also probed by Western blot for the 6x-histidine tag on NLL-MetRS.

only in the base of structures, close to the glass coverslip. Wild-type cells exhibited minimal background fluorescent signal (Figure 4.2A).

To evaluate our ability to detect proteins preferentially expressed by the labeled subpopulation, we compared proteomes enriched from P_{trc}*:nll-mc* and P_{rpoS}*:nll-mc* strains. To obtain adequate protein yield, biofilms of each strain were grown for four days in silicone tubing and treated with Anl for 1.5 h. We verified Anl incorporation in cell lysates via SDS-PAGE (Figures 4.S2A), reacted lysates with DBCO-biotin (Figures 4.S2B), enriched proteins on streptavidin beads, and analyzed proteins via LC-MS/MS. We detected 908 total proteins among two replicates from each strain. Proteins enriched from P_{rpoS}*:nll-mc* made up a subset of total protein identifications (80%) (Figure 4.2B). Based on fluorescence and Western blot detections (Figure

4.S2A-B), Anl incorporation was not significantly lower in these samples, so the decreased complexity of the sample is likely due to the targeted analysis of a subset of cells. For proteins identified from both strains, we quantified their relative abundances using label-free quantification (LFQ) and found 15 and 24 proteins to be at least two-fold more or less abundant in the P_{rpoS}*:nll-mc* strain, respectively (Figure 4.2C). Combined with proteins uniquely identified from either strain, a total of 24 and 206 proteins were more abundant in the *rpoS* or *trc* samples, respectively. Full proteomic results are listed in Dataset 4.1.

To take a functional view of region-specific expression profiles, we categorized proteins by their PseudoCAP classification [32] and searched for categories that were significantly overrepresented in each list of "hits" compared to all proteins identified. Proteins classified as transcriptional regulators were significantly more abundant in the trc sample, a set that includes regulators involved in low oxygen response (Anr) [33], quorum sensing (LasR) [34], flagellin synthesis (FliA) [35], and the global regulator Vfr [36]. A protein of particular interest is AmgR, a response regulator whose deletion causes increased sensitivity to the clinical aminoglycoside tobramycin [37].

We found ribosomal proteins to be significantly less abundant in the *rpoS* region ($p < 0.05$); the median relative abundance of 36 quantified ribosomal proteins was 0.8 fold lower in *rpoS* samples compared to the *trc* samples (Figure 4.2D, Figure 4.S2C). Furthermore, the protein with the lowest relative abundance in the *rpoS* samples was ribosomal protein RpmC (protein L29 of the 60S subunit, 22-fold less abundant). These results are consistent with measurements showing greater translational activity in upper regions of flow cell biofilms [38] and the higher levels of ribosomal transcripts in the region containing metabolically active cells found in a microarray comparison of regions within colony biofilms [13].

Of the few proteins significantly more abundant in the rpoS sample, more than half were annotated as hypothetical, unclassified, or unknown, a significant enrichment of that PseudoCAP classification as compared to all identified proteins. The proteins found whose functions are known include those involved in antibiotic resistance, stress protection, and alginate regulation (highlighted in Figure 4.2C). MltF, annotated as PA14_15720, was the protein most enriched in the rpoS subpopulation and is known to play a role in resistance to the β-lactams piperacillin, cefotaxime and ceftazidime; disruption of the gene leads to reduced minimum inhibitory concentrations for each antibiotic in planktonic cultures [39]. Biofilm resistance to β-lactams

has been linked previously to the upregulation of the β-lactamase AmpC by peripheral cells in response to antibiotic treatment [8]. The identification of MltF in the absence of antibiotic stimulation and within the biofilm interior, gives evidence for a complementary approach to tolerance in which cells are preemptively prepared for antibiotic stress. We also identified Dps, a nonspecific DNA-remodeling protein that confers protection against a variety of stresses, including starvation, peroxide treatment, UV irradiation, and others [40, 41]. In *E. coli*, *dps* transcription is RpoS dependent, and Dps is one of the most abundant proteins in stationary phase cells [42].

Another DNA binding protein, AlgP, is one of many known regulators that control synthesis of the exopolysaccharide alginate [43]. Alginate synthesis is not required for biofilm formation in vitro [44] but its upregulation is one of the hallmarks of the "mucoid" phenotype observed in some CF isolates. Besides its structural role as a component of the extracellular polymeric substance (EPS) that surrounds biofilm cells, alginate may play a role in defense against inflammation caused by host cells in the CF lung [43]. To validate the ability of our targeted proteomics approach to provide information about region-specific protein expression, we generated a strain that expresses GFP under control of the *algP* promoter (P_{algP}*:gfp*). After four days of growth, GFP fluorescence in P_{algP}*:gfp* biofilms was localized to cells within the biofilm interior (Figure 4.2D). This pattern of expression matched the localization of GFP fluorescence in P_{rpoS}*:gfp* biofilms and the localization of Anl labeleing observed in P_{rpoS}*:nll-mc* (Figure 4.2A).

As a caveat, we note that RpoS itself was equally abundant in the *rpoS* and *trc* samples. The design of the expression cassette in P_{rpoS}*:nll-mc* places NLL-MetRS under transcriptional control of any regulatory regions that lie 1 kb upstream of the endogenous *rpoS* gene. However, much of the control of RpoS protein levels is known to be post-transcriptional, depending on the action of sRNAs, modified translation rates, and tuned degradation [45]. Additionally, NLL-MetRS has a C-terminal fusion to mCherry which may increase its intracellular stability and may further disconnect levels of the mutant synthetase and RpoS itself. We conclude that P_{rpoS}*:nll-mc* cells with high levels of NLL-MetRS are not necessarily cells with high levels of RpoS protein. However, our imaging results from planktonic and biofilm growth states show that the P_{rpoS}*:nll-mc* strain can be used to target proteomic analysis to the cellular subpopulation of interest.

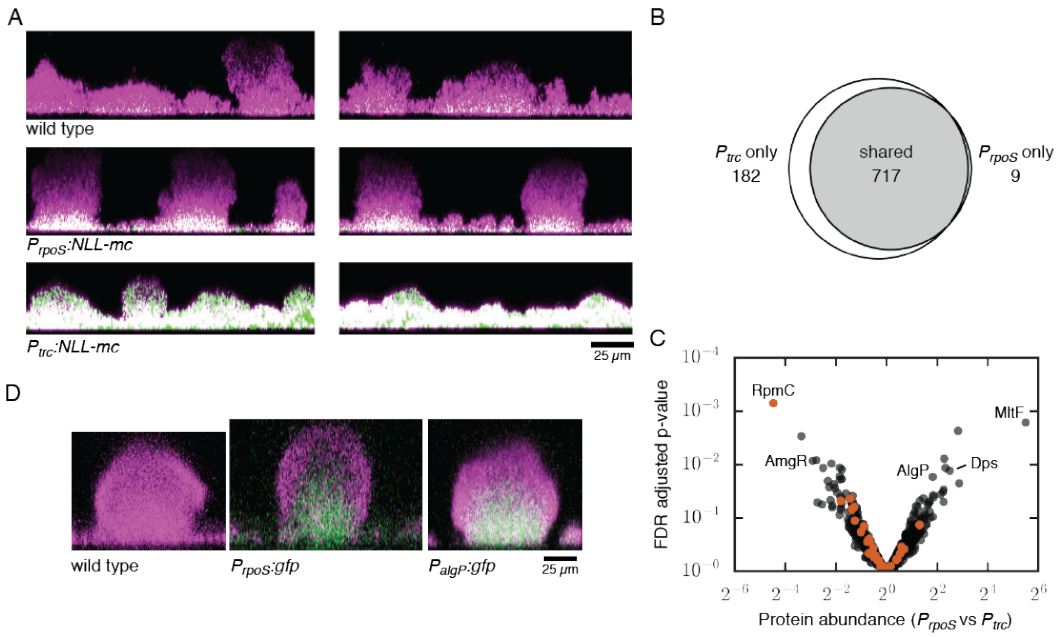

Figure 4.2: **Targeted proteomics of a biofilm subpopulation.** (A) Anl incorporation in wild-type, P_{rpoS}*:nll-mc*, and P_{trc}*:nll-mc* biofilms was visualized by reacting fixed biofilms with DBCO-TAMRA (green). Biofilms were counter stained with STYO9 (magenta). Colocalization of fluorescent signals is displayed as white. Cross-sections were reconstructed from confocal image stacks. (B) Proteins identified following BONAT enrichment from P_{rpoS}*:nll-mc* and P_{trc}*:nll-mc* strains. (C) Quantification of relative protein abundances for proteins found following enrichment from both strains. Ribosomal proteins are shown in orange. Proteins discussed in the text are indicated by name. (D) Spatial distribution of GFP expression under control of the *rpoS* or *algP* promoters in live biofilms. GFP is shown in green and SYTO62 counterstain in magenta.

BONCAT Enrichment of Proteins Throughout Ciprofloxacin Treatment.

To identify the subpopulation-specific response to ciprofloxacin, we designed an experiment to capture dynamic changes to the proteome throughout the course of antibiotic challenge. Fluorescent imaging of biofilms treated with ciprofloxacin has shown a progression of cell death over the course of 13 h [6]. Cell death, visualized by propidium iodide staining, began between 4 and 9 h of treatment, and was restricted to peripheral regions of biofilm microstructures. Protein synthetic activity, measured by detection of expression of an unstable GFP variant, continued in interior biofilm populations even after 13 h of treatment. We replicated this time course of antibiotic challenge by treating four day-old P_{rpoS}*:nll-mc* biofilms with ciprofloxacin. To achieve temporal selectivity, we pulse-labeled biofilms with Anl at 0, 4, or 13 h after ciprofloxacin was added. Each pulse was for 1.5 h to distinguish

newly synthesized proteins from the preexisting proteome. To serve as a "no cipro." control, we also labeled untreated biofilms for 1.5 h with Anl (Figure 4.3A).

We tracked the number of viable cells recovered from biofilms throughout the time course of treatment and found two stages of killing (Figure 4.3B). Compared to the untreated control, biofilms treated for 1.5 or 5.5 h exhibited an approximately 50-fold loss in viable cells, while those treated for 14.5 h exhibited a 500-fold loss. Treatment with Anl had no effect on the number of viable cells. In contrast, levels of Anl incorporation from the same samples showed a decrease with longer ciprofloxacin treatment, but varied less than two-fold (Figure 4.3C). This apparent discrepancy between viable cell counts and protein synthetic activity is likely due to a number of factors. Since we have shown that the P_{rpoS}*:nll-mc* strain allows targeted labeling of a small subpopulation of biofilm cells in the region known to tolerate ciprofloxacin treatment, we expect that cells incorporating Anl will be viable throughout treatment. Second, viability counts by plating do not necessarily reflect the number of translationally active cells, exemplified by the body of literature documenting so called viable but non-culturable cells [46] particularly in the context of antibiotic persistence [47]. Finally, the total amount of Anl incorporation in a given time is dependent on both the number of translationally active cells as well as the overall rate of translation, as shown above for P_{rpoS}*:nll-mc* labeling in planktonic cultures; a lower level of Anl incorporation reflects either a reduction in active cells, a reduction in the protein synthesis of those cells, or some combination.

We performed BONCAT enrichment on lysates from each experimental condition (performed in triplicate) and identified proteins by LC-MS/MS. We identified more than 1200 proteins among all runs. Protein abundances, estimated by LFQ, were well correlated between experimental replicates (Figure 4.3D). We used principal component (PC) analysis to visualize the variance among replicates and experimental conditions (Figure 4.3E) and found that, in general, biological replicates clustered with one another and that ciprofloxacin treated samples were separated from the untreated control samples. For each time point, we quantified differences in protein abundances compared to the untreated control (Figure 4.3F). Consistent with the correlation analysis, fewer proteins were significantly changed in the 1.5 h treatment condition (73 proteins) than in the 5.5 h (187 proteins) or 14.5 h (204 proteins) treatment conditions (Figure 4.S3). Correlation, PC, and quantification analyses are consistent with the classification of the proteomic data into two subgroups: proteins whose rates of synthesis change immediately upon ciprofloxacin

exposure, and a later response characterized by a greater number of changes, many of which are shared between the 5.5 h and 13.5 h groups.

For the following analyses, we subset proteins identified at each time point into groups significantly more or less abundant in the treated vs. untreated control. Each group includes proteins whose relative abundances were quantified (fold-change > 2 and FDR adjusted p-value < 0.05) as well as proteins identified in one condition (at least two of three replicates) and not identified in the other (not found in any replicates). Full proteomic results are listed in Dataset 4.2.

The Dynamic Proteomic Response to Ciprofloxacin.

We first compared our results to other studies of the *P. aeruginosa* response to ciprofloxacin. The responses of planktonic *P. aeruginosa* to sub-MIC to supra-MIC ciprofloxacin treatments (0.01 to 1.0 μg/mL) have been characterized via microarray measurements of transcript abundances [10, 48, 49]. While the design of these experiments differed, a small consensus of responses to ciprofloxacin has emerged. These changes include the upregulation of proteins involved in the SOS response and DNA repair (e.g., RecA) and the pyocin synthesis regulator, PrtN. We found that our dataset generally matched these reported changes; RecA, PrtN, the negative regulator of type III secretion, PtrB (PA14_07970), and the ribonucleotide reducatase complex (NrdAB) were either significantly upregulated or uniquely identified in the treated samples (Figure 4.S4A).

As described above, early and late responses differed in our dataset. In fact, only three proteins were significantly upregulated at all times: the DNA gyrase GyrB, a direct target of ciprofloxacin; the protein chaperone HscK; and the methylisocitrate lyase PrpB. These proteins typify functional categories of proteins we found to be upregulated by ciprofloxacin challenge, namely those involved in remediating DNA damage and other stress, and proteins involved in central metabolism.

Ciprofloxacin inhibits DNA gyrase activity, causing DNA damage during replication attempts. DNA damage leads to an induction of the SOS response, characterized by depletion of the SOS repressor LexA and the resulting upregulation of genes that alleviate DNA damage stress [50]. We did not identify LexA in any experiments, but we detected upregulation of the LexA target RecA which binds to DNA lesions. Of the proteins involved in DNA damage response and repair found in our dataset, all were either significantly upregulated or uniquely identified in at least one time point (Figure 4.4A, Figure 4.S4B). This set includes both subunits of DNA gyrase

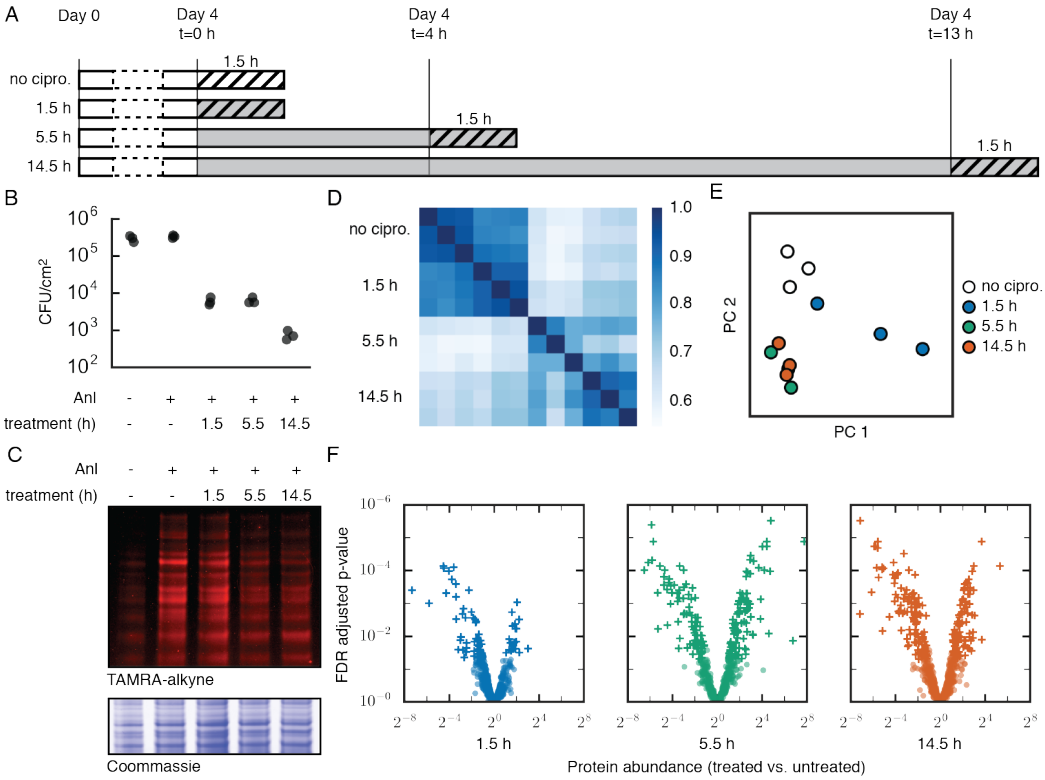

Figure 4.3: **BONCAT analysis of protein synthesis during ciprofloxacin challenge.** (A) Experimental timeline of biofilm treatment and proteome labeling. Biofilms were grown in silicone tubing for four days and then treated with ciprofloxacin (gray bars). Control biofilms were untreated. For each experimental condition, biofilms were treated with Anl at the designated time point for 1.5 h (cross hatch) and then lysed. (B) Survival of biofilm cells following treatment with 60 µg/mL ciprofloxacin for the indicated time. (C) Visualization of Anl incorporation. (D) Spearman rank correlation coefficients for protein LFQ values, calculated among all MS runs. (E) Coordinates for each MS run in two dimensional principal component space. (F) Protein abundance fold changes for each experimental condition compared to the ciprofloxacin untreated control. Proteins that are significantly more or less abundant are shown as crosses (FDR adjusted p-value < 0.05 and fold change > 2).

(GyrA and GyrB), the direct target of ciprofloxacin; and proteins involved in sensing (RecA, UvrA) and repairing (RecB, RecQ, MutM) various types of DNA damage.

The differences between early and late responses are best exemplified by the contrasting behavior of proteins involved in flagella synthesis and purine metabolism. Protein components of flagella and flagellar regulation were significantly upregulated throughout the course of ciprofloxacin treatment including the immediate upregulation of FliC, FliM, and FlgM (Figure 4.4B). Flagella are known to con-

tribute to the development of biofilm microstructures. Specifically, strains deficient in flagellar synthesis are unable to colonize the upper regions of flow cell biofilms [51]. At the 14.5 h time point, only FleN remains upregulated.

In contrast, many proteins involved in purine metabolism are upregulated only at the 4.5 and 14.5 h time points (Figure 4.4C). Of the proteins in the pathway for *de novo* synthesis of inosine monophosphate (IMP) that we identified (PurBDEFHLMT), four of eight were significantly upregulated in at least one of the later time points. PurA, required for IMP's conversion to the ribonucleotide adenosine monophosphate, was likewise upregulated. The ribonucleotide reducatase complex (NrdA and NrdB) that generates deoxyribonucleotides from their ribonucleotide precursors was also upregulated.

Finally, some of the largest changes we observed were the up- and downregulation of proteins involved in central metabolism. These include many components of the citrate (tricarbyoxylic acid, TCA) (Figure 4.4D) and methylcitrate cycles (Figure 4.S4C). We found slight upregulation of the isocitrate lyase, AceE, which catalyzes the first step in the glyoxylate shunt, a metabolic pathway previously shown to be important for *Burkholderia cepacia* persistence to antibiotics *in vitro* [52] and the persistence of *Mycobacterium tuberculosis* in mice [53]. Of particular interest is the differential behavior of the aconitases and isocitrate dehydrogenases (ICD). The *P. aeruginosa* genome encodes two of each protein class (aconitases AcnA and AcnB and ICD's Icd and Idh). We found AcnA to be significantly downregulated and AcnB significantly upregulated in the later response conditions. Similarly, expression of Icd, the monomeric ICD was unchanged, while the dimeric Idh was the protein most upregulated at the 14.5 h time point.

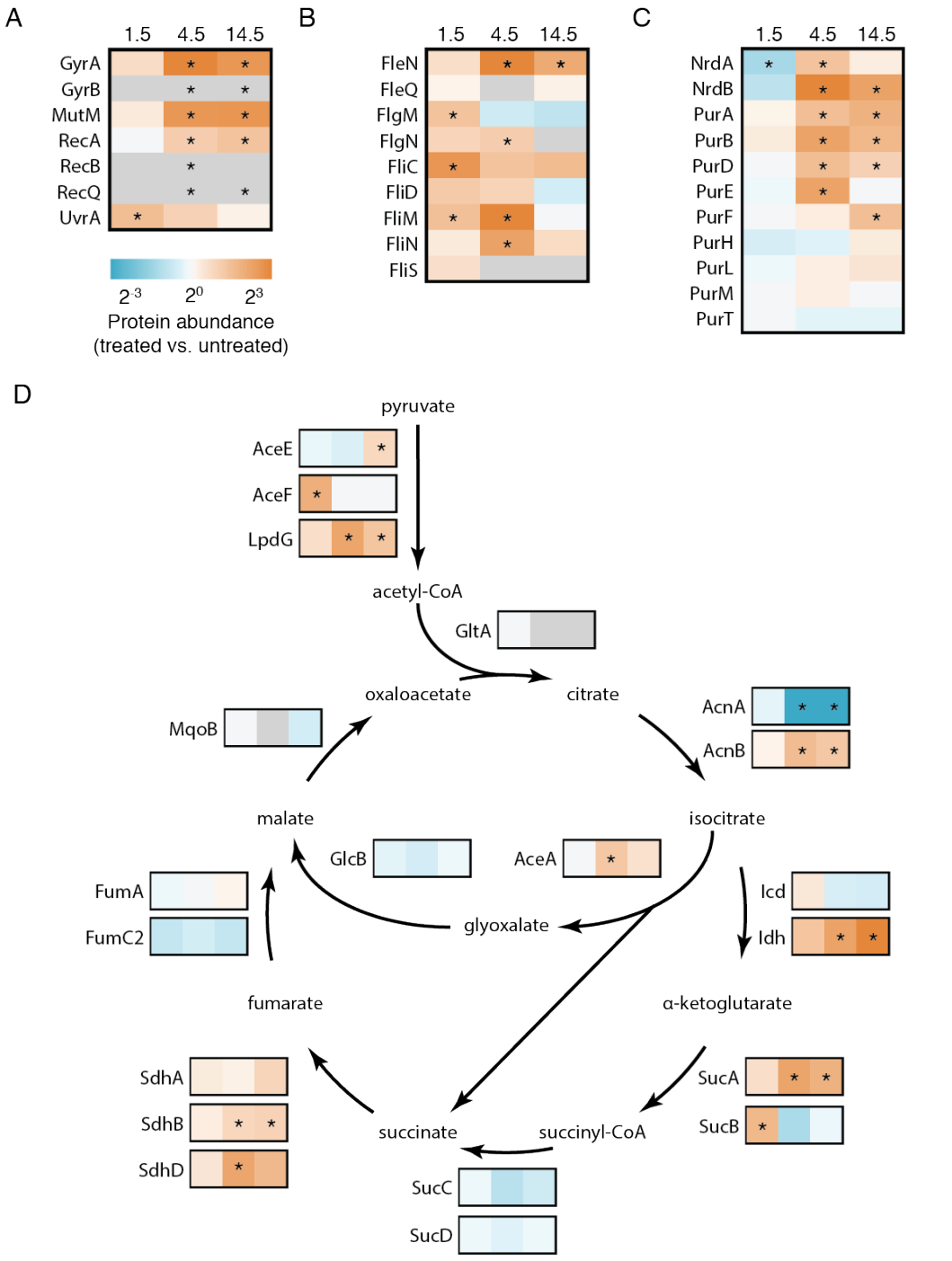

Figure 4.4: **Dynamic cellular responses to ciprofloxacin.** Heatmaps indicating changes in abundance at each time point as compared to the untreated control for proteins involved in (A) DNA damage and repair, (B) flagella synthesis, (C) purine metabolism, and (D) the TCA cycle and glyoxalate shunt. The color scale for abundance ratios is shown under panel (A). Gray boxes represent proteins that were not quantified. Asterisks indicate abundance ratios that were significantly different from 1 (FDR adjusted p-value < 0.05) or proteins that were identified in the treated sample but not in the untreated control (gray with an asterisk).

4.4 Discussion

Here we introduce an adaptation to the BONCAT method that allows for selective proteomic analysis of a phenotypic subpopulation in genotypically identical bacterial cultures. Our approach for targeting protein labeling to a subset of cells is generally applicable toward the study of heterogeneous systems (e.g., planktonic persister cells, or *in vivo* infections), and we show that the use of endogenous regulatory elements allows precise control over the targeted phenotype. For our studies of biofilms, we found that the *rpoS* promoter allowed for targeting of biofilm interiors, but we note that the approach is general and that, in principle, any genetic regulatory element can be used to target other subpopulations within biofilms or other systems.

In the context of biofilm antibiotic tolerance, we show that targeted labeling with Anl allows for detection of protein synthesis after extended incubation with a supra-MIC of ciprofloxacin, and through enrichment and LC-MS/MS analysis of labeled proteins, we detect and differentiate the immediate response and the long-term adaptation to antibiotic stress. We find congruence with previously reported responses to ciprofloxacin by planktonic *P. aeruginosa*, including upregulation of key components of the SOS response to DNA damage and the two subunits of DNA gyrase, a direct target of the drug. Our proteomic dataset encompasses a variety of other responses, including the immediate upregulation of proteins for flagellar motility, and the delayed upregulation of purine synthesis proteins.

Some of the most striking changes were the rearrangement of proteins involved in the central carbon metabolism. The 2-methylisocitrate lyase PrpB is one of the few proteins upregulated by ciprofloxacin at all three time points, and the dimeric ICD Idh shows the highest fold upregulation following 14.5 h of treatment. We also find upregulation of various other proteins involved in the citrate and methylcitrate cycles, and interestingly, differential expression of proteins that can perform the same enzymatic activity: the ICDs Idh (upregulated) and Icd (unchanged), and the aconitases AcnA (downregulated) and AcnB (upregulated). To our knowledge, broad adjustments to central carbon metabolism in *P. aeruginosa* biofilms have not been reported as a mechanism for antibiotic tolerance or adaptation. However, changes in TCA cycle enzymes and intermediate metabolites have been discussed for their role in maintaining redox conditions in response to reactive oxygen species (ROS). Although linked to the somewhat controversial claim that ROS is the primary and general mechanism for antibiotic-induced killing, genetic experiments have shown that the deletion of some but not all TCA cycle enzymes (acnonitase and ICD

genes in particular) confer increased resistance to *E. coli* treated with antibiotics, presumably through the adjustment of the intracellular NAD+/NADH balance [54].

The role of central carbon metabolism in the response to antibiotic stress has been studied more thoroughly in *Mycobacterium tuberculosis* (Mtb), another organism that chronically infects the human lung. Measurements of TCA cycle metabolites showed that treatment of Mtb with a variety of antibiotics leads to the increased abundance of pyruvate, succinate, and fumarate [55]. Though we didn't perform metabolomic measurements, the proteomic changes we observe are consistent with changes to these metabolites. Upregulation of components of the pyruvate dehydrogenase (AceEF and LpdG) and succinate dehydrogenase (SdhABC) complexes are consistent with increased flux from pyruvate, and from succinate to fumarate respectively. The role of the methylcitrate cycle in infection has also been investigated in Mtb, where it is required for growth within macrophages (an environment with high levels of ROS) [56]. From our dataset, PrpB (upregulated) catalyzes the generation of methylcitrate, and in *E. coli* AcnB (upregulated), but not AcnA (downregulated), has activity toward methylcitrate in addition to its canonical role as a citrate aconitase [57]. We caution that even core central metabolism can differ substantially among bacteria, but that there is precedent for a critical role of central carbon metabolism in general stress responses.

Our measured proteomic responses of a *P. aeruginosa* biofilm subpopulation lead to interesting questions about the roles of these proteins in ciprofloxacin tolerance. To what extent are changes to the central carbon proteome important for their effects on general redox balance vs. their effects on intermediate metabolite concentrations? What is the physiological benefit of the differential expression of redundant enzymes like the aconitases and ICDs? Dissecting the roles of these proteins and others in the data set through focused genetic experiments and metabolomics should provide better understanding of these phenomena. In addition, our temporal analysis suggests that there are important differences between immediate responses and longer term physiological adaptations. Finally, this method for selective proteomics is readily applicable for the study of subpopulation-specific responses to other stresses (e.g., antibiotics with other mechanisms of action).

4.5 Experimental Procedures

Strain construction. All strains are listed in Table 4.1. We used standard cloning procedures. Enzymes were purchased from New England Biolabs. For chromosomal integration into the *Tn7* site, pUC18T mini-Tn7T [58] was modified with the desired expression cassette, followed by tetraparental conjugation to the PA14 host strain. Genomic DNA was prepared using the GenElute Bacterial DNA kit (Sigma-Aldrich). The 1 kb regions upstream of *rpoS* and *algP* were amplified from *P. aeruginosa* genomic DNA. GFP-expressing cassettes contain the gene for *gfp*mut3b, cloned from pBK-mini-Tn7-gfp2 [59]. The gene encoding the *E. coli* mutant methionyl-tRNA synthetase was cloned from plasmid pJTN1 [28]. A shuttle vector allowing for arabinose-inducible expression of NLL-MetRS was created by cloning the gene from pJTN1 into pBAD18 [60] and then ligation of the fragment containing *araC* and P_{ara}*:nll* into pUCP24 [61] to generate pBADP-NLL. *P. aeruginosa* was transformed by electroporation.

Media and growth conditions. Planktonic cultures were grown at 37 °C with shaking. Liquid media were LB (5 g yeast extract, 10 g tryptone, 10 g NaCl per liter), or FAB with 0.05 g/L glucose (for biofilms) or 5 g/L glucose (for planktonic cultures) in place of citrate for biofilms [63]. For confocal imaging, biofilms were grown in flow cells (1x4x40 mm) (Stovall) as previously described [64], but without bubble traps. Biofilms were grown at 37 °C with a constant flow rate of 0.03 mL/min. For proteomic analyses, biofilms were grown in silicon tubing (10 mm interior diameter, 20 cm long) (McMaster-Carr) at 37 °C with a constant flow rate of 0.5 mL/min, as previously described [65]. Loosely adherent biofilm cells were extracted by collecting media within each tube and flushing with 0.9% NaCl. Tubing was cut into 1 cm pieces and vortexed in 0.9% NaCl to remove all cells.

BONCAT labeling and enrichment. For planktonic labeling experiments, strains were diluted from overnight cultures 1:100 into FAB medium with 5 g/L glucose. At each time point, labeling was initiated by the addition of 1 mM Anl (Iris-Biotech). The strain containing pBADP-NLL-MetRS was grown in the presence of 50 µg/mL gentamicin and treated with 1 mM Anl and 20 mM arabinose. For all, after 15 min of incubation with Anl at 37 °C with shaking, cells were pelleted at 4 °C, washed once with ice cold 0.9% NaCl and frozen at -80 °C. For biofilm experiments, flow was stopped and tubing was clamped. FAB medium with 0.05 g/L glucose and 1 mM Anl was injected by syringe and biofilms were incubated for 1.5 h at 37 °C. For

Table 4.1: **Chapter 4: Strains and plasmids.** Strains and plasmids used in this study. Plasmids are stored as *E. coli* strains carrying the plasmid, and requests should be for the *E. coli* strain.

***Pseudomonas aeruginosa* Strains**		
Name	Genotype	Source
DKN263	*P. aeruginosa* UCBPP-PA14	
BMB1	UCBPP-PA14 attTn7::mini-Tn7T-Gm^R P_{rpoS}*:gfp*	This Study
BMB2	UCBPP-PA14 attTn7::mini-Tn7T-Gm^R P_{trc}*:gfp*	This Study
BMB3	UCBPP-PA14 attTn7::mini-Tn7T-Gm^R P_{rpoS}*:nll-mc*	This Study
BMB4	UCBPP-PA14 attTn7::mini-Tn7T-Gm^R P_{trc}*:nll-mc*	This Study
BMB5	UCBPP-PA14 attTn7::mini-Tn7T-Gm^R P_{algP}*:gfp*	This Study
***Escherichia coli* Strains**		
Name	Genotype	Source
DKN1299	SM10, pTNS1	[58]
DKN1299	HB101 pRK2013	[58]
BMB6	Mach1 pUC18T-mini-Tn7T-Gm^R P_{rpoS}*:gfp*	This Study
BMB7	Mach1 pUC18T-mini-Tn7T-Gm^R P_{trc}*:gfp*	This Study
BMB8	Mach1 pUC18T-mini-Tn7T-Gm^R P_{rpoS}*:nll-mc*	This Study
BMB9	Mach1 pUC18T-mini-Tn7T-Gm^R P_{trc}*:nll-mc*	This Study
BMB10	Mach1 pUC18T-mini-Tn7T-Gm^R P_{algP}*:gfp*	This Study
BMB11	Mach1 pUCP18	[62]
BMB12	Mach1 pBAD18-NLL-MetRS	This Study
BMB13	Mach1 pBADP-NLL-MetRS	This Study

proteome analysis, cells were collected from tubing as described above, pelleted, and frozen at -80 °C.

All samples were lysed by resuspension in lysis buffer (100 mM Tris-HCl, pH 8, 4% SDS). Lysates were sonicated with a microtip probe for 30 s at setting 20% (Qsonica). For fluorescence detection of Anl-labeled proteins, lysates were reacted with 5 µM TAMRA-alkyne (Click Chemistry Tools), 100 µM $CuSO_4$, 500 µM tris(3-hydroxypropyltriazolylmethyl)amine (THPTA), 5 mM aminoguanidine hydrochloride, and 5 mM sodium ascorbate for 15 min at room temperature [66]; precipitated with water, methanol, and chloroform; and washed twice with methanol. Reacted lysates were separated via SDS-PAGE and imaged on a Typhoon gel imager (GE Healthcare). Gels were stained with Colloidal Blue (Life Technologies) or Instant-

Blue (Expedeon) Coomassie stains to verify equal protein loading.

For all enrichments, cysteines were reduced by addition of 10 mM dithiothreitol (DTT) for 20 min at room temperature and alkylated by addition of 100 mM chloroacetamide for 30 min in the dark. For the comparison between P_{rpoS}*:nll-mc* and P_{trc}*:nll-mc* biofilms, 0.5 mg of protein lysate per sample were reacted with 12 µM DBCO-sulfo-biotin (Click Chemistry Tools) in 0.5 mL PBS for 15 min at room temperature. Proteins were precipitated with acetone at -20 °C and resuspended in PBS, 0.3% SDS. Streptavidin UltraLink Resin (Pierce Biotechnology) was washed twice with PBS, added to biotinylated lysates, and incubated overnight at 4 °C. Resin was transferred to microfuge spin columns (Pierce Biotechnology) and washed twice with 1% SDS in PBS and once with 0.1% SDS in PBS. Proteins were eluted by incubation with 1 mM biotin at 65 °C for 20 min. Eluted proteins were separated via SDS-PAGE (4-12% Bis-Tris gradient gel, Thermo Fisher) and subjected to GeLCMS.

For the comparison between ciprofloxacin treated samples, reduced and alkylated lysates (0.5 mg per sample) in 0.5 mL PBS were reacted with 50 µL of DBCO-agarose bead 50% slurry (Click Chemistry Tools) for 2.5 h at room temperature. Beads were washed extensively in gravity flow columns (Bio-Rad) with 40 mL each of PBS, 0.8% (w/v) SDS; 8 M urea; and 20% (v/v) acetonitrile in water. Beads were resuspended in 50 mM ammonium bicarbonate (AB) for on-bead tryptic digestion (see LC-MS/MS section for details).

Imaging flow cell biofilms. All treatments were applied via syringe to flow cell biofilms. For GFP imaging, flow was stopped and live biofilms were incubated with 0.05 µM SYTO 62 (ThermoFisher) for 30 min at 37 °C. To visualize Anl incorporation, biofilms were fixed by incubation with 3.7% formaldehyde for 30 min and permeabilized by incubation with 70% ethanol for 5 min on ice. Fixed biofilms were washed with 0.9% NaCl, incubated with 100 mM chloroacetamide in the dark for 30 min, and treated with 25 µM DBCO-TAMRA (Click Chemistry Tools) in PBS for 30 min. Biofilms were washed extensively to remove excess dye and counter stained with 0.05 µM STYO 9 (ThermoFisher).

LC-MS/MS For GeLCMS, gel lanes were cut into 8 pieces each and destained by alternating washes with 50 µL each of 50 mM ammonium bicarbonate (AB) and 1:1 50 mM AB:acetonitrile. Proteins were reduced by incubation with 6.7 mM dithiothreitol (DTT) in 50 µL 50 mM AB at 50 °C for 30 min and alkylated by incubation with 37 mM iodoacetamide in 50 µL 50 mM AB at room temperature for

20 min. Gel pieces were washed with 50 µL each of 100 mM AB and acetonitrile. Proteins were digested with 300 ng endoproteinase LysC in 50 µL 100 mM Tris-HCl at 37 °C for 18 h. Peptides were extracted by sequential washing with: 50 µL each of 1% formic acid/2% acetonitrile, 1:1 acetonitrile:water, and 1% formic acid in acetonitrile. Peptides were desalted with C18 ZipTips (EMD Millipore).

For on-bead digestion following enrichment, agarose beads were incubated with 100 ng trypsin in 9:1 AB:acetonitrile for 18 h at 37 °C. Supernatant was collected and beads were washed twice with 20% acetonitrile to extract all peptides. Peptides were dried, passed through HiPPR spin columns (ThermoFisher) to remove any residual SDS, and desalted with C18 ZipTips.

Liquid chromatography-mass spectrometry experiments were essentially carried out as previously described [67]. The *rpoS* vs. *trc* experiments were performed on a nanoflow LC system, EASY-nLC 1000 coupled to a hybrid linear ion trap Orbitrap Classic mass spectrometer (Thermo Scientific) equipped with a nanoelectrospray ion source (Thermo Scientific) with the following modifications: For the EASY-nLC II system, solvent A consisted of 97.8% H_2O, 2% ACN, and 0.2% formic acid and solvent B consisted of 19.8% H_2O, 80% ACN, and 0.2% formic acid. For the LC-MS/MS experiments, digested peptides were directly loaded at a flow rate of 500 nL/min onto a 16-cm analytical HPLC column (75 µm ID) packed in-house with ReproSil-Pur C_{18}AQ 3 µm resin (120 Å pore size, Dr. Maisch, Ammerbuch, Germany). The column was enclosed in a column heater operating at 30 °C. After 30 min of loading time, the peptides were separated with a 50 min gradient at a flow rate of 350 nL/min. The gradient was as follows: 0–30% B (50 min), and 100% B (10 min). The Orbitrap was operated in data-dependent acquisition mode to automatically alternate between a full scan (m/z=400–1600) in the Orbitrap and subsequent 10 CID MS/MS scans in the linear ion trap. CID was performed with helium as collision gas at a normalized collision energy of 35% and 30 ms of activation time. Ciprofloxacin experiments were performed on a hybrid ion trap-Orbitrap Elite mass spectrometer (Thermo Scientific).

Raw files were searched using MaxQuant [68] against the *P. aeruginosa* PA14 UniProt entries (5,886 sequences) and a contaminant database (246 sequences). Trypsin was specified as the digestion enzyme with up to two missed cleavages. Carbamidomethylation of cysteine was set as a fixed modification and protein N-terminal acetylation and methionine oxidation were variable modifications. Protein abundances were estimated with MaxLFQ [69], and for each experiment, peptides

were matched between runs. LFQ values were normalized and used to calculate abundance ratios between samples and to estimate variance using the limma package in R [70]. P-values were adjusted for false discovery by the Benjamini-Hochberg procedure [71].

Software analysis and data presentation. This section describes software packages that were not mentioned above. Data processing and statistical analysis were performed with Python version 2.7.9 with NumPy version 1.9.2, SciPy version 0.15.1, and Pandas version 0.16.1. Data were plotted with Matplotlib version 1.5.1 [72] and Seaborn version 0.7.0. Microscopy and gel images were analyzed with ImageJ 64-bit version 2.0.0 [73]. Figures were assembled in Adobe Illustrator CS5.

4.6 Supplementary Figures

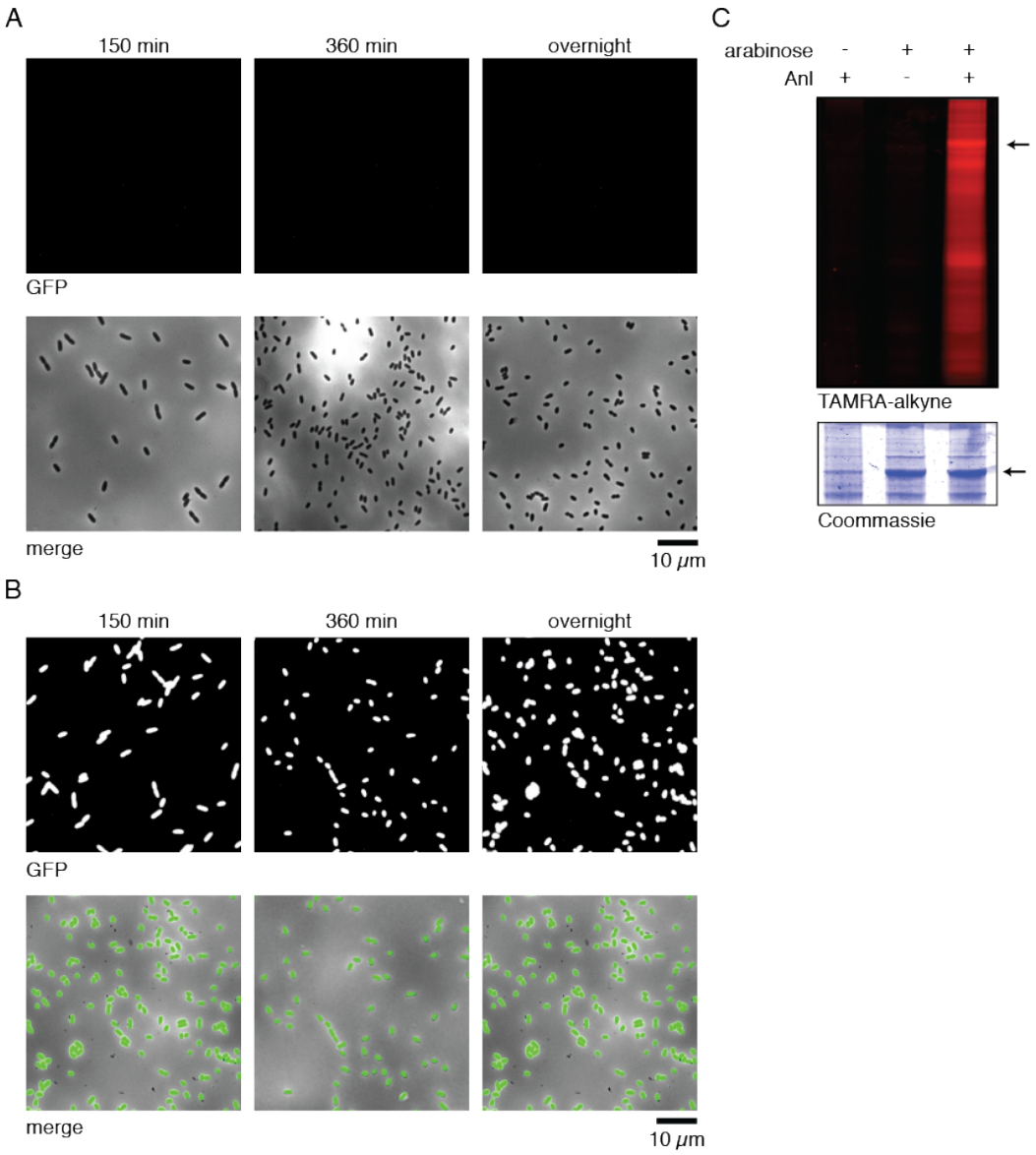

Figure 4.S1: **Promoter-controlled expression.** (A, B) Fluorescence imaging of wild type (A) and P_{trc}*:gfp* (B). GFP fluorescence (top) and GFP-bright field merge (bottom). (C) Controlled proteome labeling with inducible expression of NLL-MetRS from the *ara* promoter. SDS-PAGE gel imaged for TAMRA fluorescence (top) and stained with Coomassie (bottom). Arrows indicate the NLL-MetRS protein.

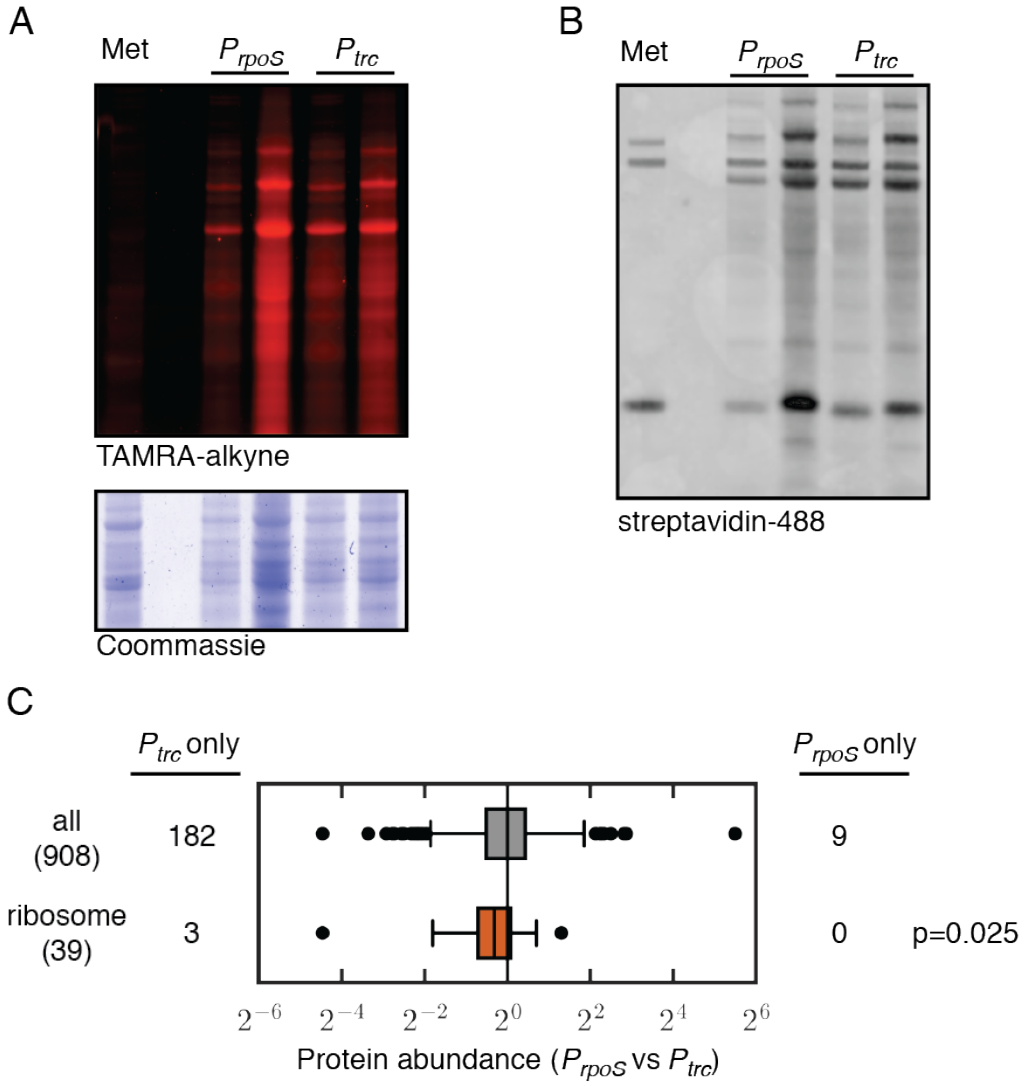

Figure 4.S2: **Enrichment from biofilms of P_{rpoS} and P_{trc} strains.** (A) SDS-PAGE gel showing Anl incorporation for each biofilm replicate. (B) Western blot with streptavidin-Alexa Fluor 488 of lysates reacted with DBCO-sulfo-biotin for affinity enrichment. Three naturally biotinylated proteins are visible in the methionine-treated negative control. (C) Distribution of protein abundance ratios for all proteins (gray) and for ribosomal proteins (orange). P-value was calculated by bootstrapped subsampling from the set of all abundance ratios (n = 1000).

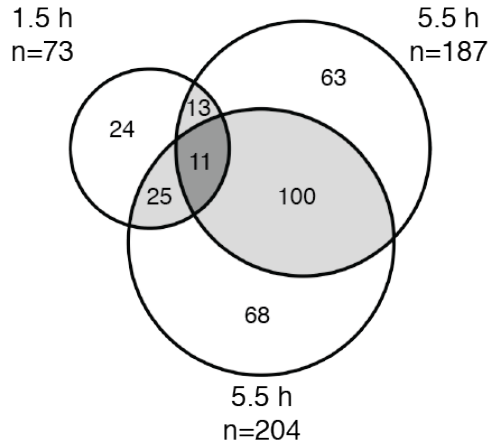

Figure 4.S3: **Shared and unique proteomic hits.** Overlap of protein hits (both down- and upregulated) at each time point throughout ciprofloxacin treatment.

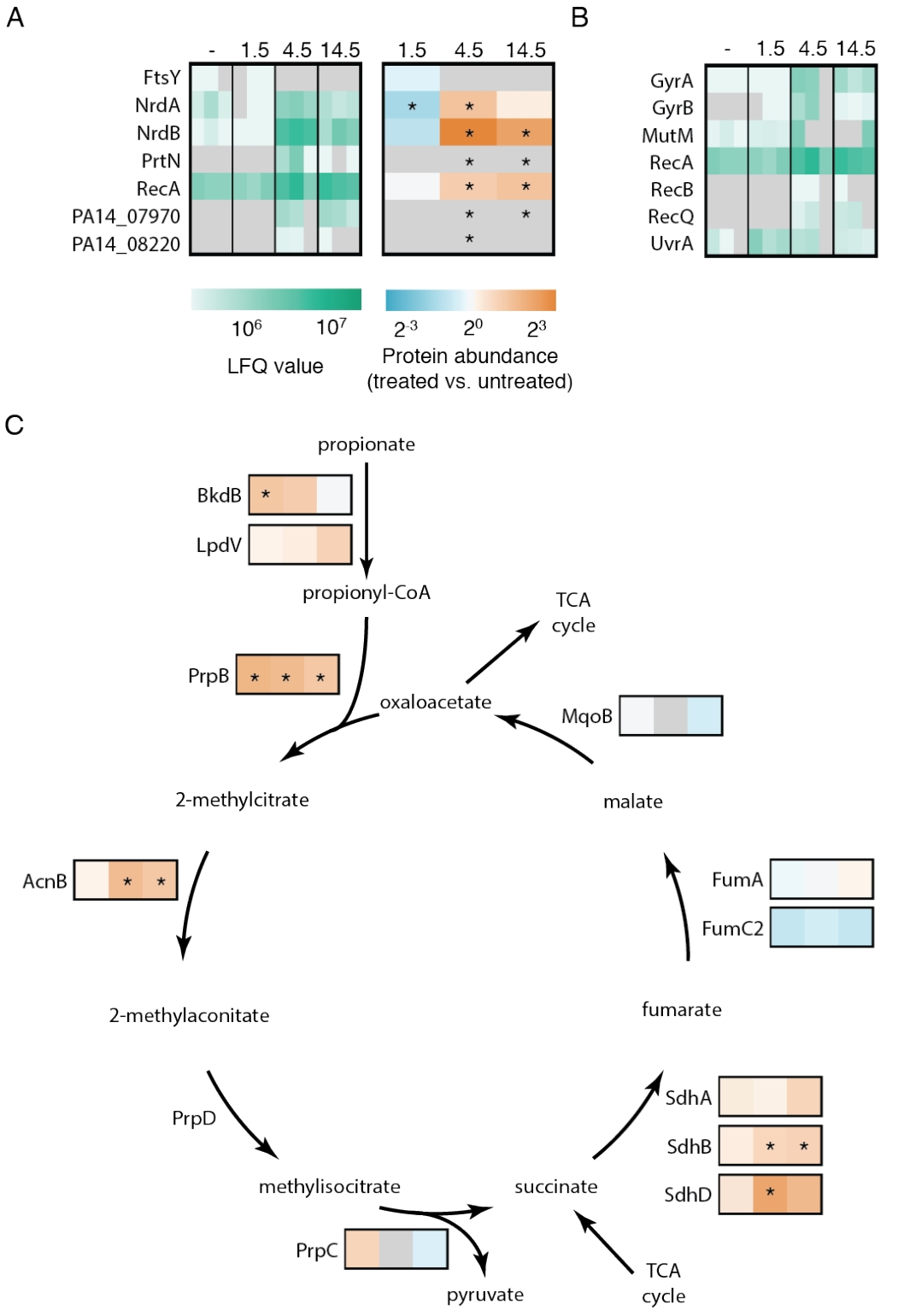
A
- 1.5 4.5 14.5
1.5 4.5 14.5
FtsY
NrdA
NrdB
PrtN
RecA
PA14_07970
PA14_08220
10^6 10^7
LFQ value
2^{-3} 2^0 2^3
Protein abundance
(treated vs. untreated)
B
- 1.5 4.5 14.5
GyrA
GyrB
MutM
RecA
RecB
RecQ
UvrA
C
propionate
BkdB
LpdV
propionyl-CoA
TCA
cycle
PrpB
oxaloacetate
MqoB
2-methylcitrate
malate
AcnB
FumA
FumC2
2-methylaconitate
fumarate
PrpD
SdhA
SdhB
SdhD
methylisocitrate
succinate
PrpC
pyruvate
TCA
cycle

Figure 4.S4: **Other responses to ciprofloxacin.** (A) LFQ values and protein abundance ratios compared to the untreated sample for genes previously reported to be upregulated in response to ciprofloxacin treatment by Cirz, et al [10]; Brazas and Hancock [48]; and Linares, et al [49]. (B) LFQ values for proteins involved in the SOS response. (C) Abundance ratios for proteins involved in the isocitrate cycle. Asterisks indicate abundance ratios that were significantly different from 1 (FDR adjusted p-value < 0.05) or proteins that were identified in the treated sample but not in the control (gray with an asterisk).

4.7 Supplementary Datasets

Dataset 4.1. Proteomic results for *trc* and *rpoS* biofilm enrichments. All proteins identified by LC-MS/MS from the BONCAT-enriched samples are listed. Column 1 gives the Uniprot ID. Columns 2-5 give the LFQ intensity values for each sample. Column 6 gives the log_2 abundance ratio (*rpoS* vs. *trc*). Column 7 gives the FDR-adjusted p-value. Columns 8-17 give the following gene identification information: PA14 locus tag, gene name if available, protein description, list of PseudoCAP annotations, GenBank gene accession number, GenBank GI number, gene name from the KEGG database, KEGG orthology number, KEGG enzyme number, PAO1 locus tag.

Dataset 4.2. Proteomic results for ciprofloxacin treated biofilms. All proteins identified by LC-MS/MS from the BONCAT-enriched ciprofloxacin experiment are listed. Column 1 gives the Uniprot ID. Columns 2-13 give the LFQ intensity values for each sample. Columns 14, 16, and 18 give the log_2 abundance ratios (treated vs. untreated) for each time point. Columns 15, 17, and 19 give the FDR-adjusted p-values for each ratio. Columns 20-29 give the following gene identification information: PA14 locus tag, gene name if available, protein description, list of PseudoCAP annotations, GenBank gene accession number, GenBank GI number, gene name from the KEGG database, KEGG orthology number, KEGG enzyme number, PAO1 locus tag.

References

(1) Fux, C. A.; Costerton, J. W.; Stewart, P. S.; Stoodley, P. *Trends Microbiol.* **2005**, *13*, 34–40.

(2) Levin, B. R.; Rozen, D. E. *Nat. Rev. Microbiol.* **2006**, *4*, 556–562.

(3) Oliver, A.; Cantón, R.; Campo, P.; Baquero, F.; Blázquez, J. *Science* **2000**, *288*, 1251–1254.

(4) Høiby, N.; Bjarnsholt, T.; Givskov, M.; Molin, S.; Ciofu, O. *Int. J. Antimicrob. Ag.* **2010**, *35*, 322–332.

(5) Stewart, P. S.; Franklin, M. J. *Nat. Rev. Microbiol.* **2008**, *6*, 199–210.

(6) Pamp, S. J.; Gjermansen, M.; Johansen, H. K.; Tolker-Nielsen, T. *Mol. Microbiol.* **2008**, *68*, 223–240.

(7) Walters, M. C.; Roe, F.; Bugnicourt, A.; Franklin, M. J.; Stewart, P. S. *Antimicrob. Agents Ch.* **2003**, *47*, 317–323.

(8) Bagge, N.; Hentzer, M.; Andersen, J. B.; Ciofu, O.; Givskov, M.; Høiby, N. *Antimicrob. Agents Ch.* **2004**, *48*, 1168–1174.

(9) Wu, X.; Held, K.; Zheng, C.; Staudinger, B. J.; Chavez, J. D.; Weisbrod, C. R.; Eng, J. K.; Singh, P. K.; Manoil, C.; Bruce, J. E. *Mol. Cell Proteomics* **2015**, *14*, 2126–2137.

(10) Cirz, R. T.; O'Neill, B. M.; Hammond, J. A.; Head, S. R.; Romesberg, F. E. *J. Bacteriol.* **2006**, *188*, 7101–7110.

(11) Park, A. J.; Krieger, J. R.; Khursigara, C. M. *FEMS Microbiol. Rev.* **2016**, DOI: 10.1093/femsre/fuv051.

(12) Lenz, A. P.; Williamson, K. S.; Pitts, B.; Stewart, P. S.; Franklin, M. J. *Appl. Environ. Microb.* **2008**, *74*, 4463–4471.

(13) Williamson, K. S.; Richards, L. A.; Perez-Osorio, A. C.; Pitts, B.; McInnerney, K.; Stewart, P. S.; Franklin, M. J. *J. Bacteriol.* **2012**, *194*, 2062–2073.

(14) Khemiri, A.; Jouenne, T.; Cosette, P. *Med. Microbiol. Immunol.* **2016**, *205*, 1–19.

(15) Chua, S. L.; Yam, J. K. H.; Hao, P.; Adav, S. S.; Salido, M. M.; Liu, Y.; Givskov, M.; Sze, S. K.; Tolker-Nielsen, T.; Yang, L. *Nat. Commun.* **2016**, *7*, 10750.

(16) Schwanhäusser, B.; Gossen, M.; Dittmar, G.; Selbach, M. *Proteomics* **2009**, *9*, 205–209.

(17) Dieterich, D. C.; Link, A. J.; Graumann, J.; Tirrell, D. A.; Schuman, E. M. *Proc. Natl. Acad. Sci. U.S.A.* **2006**, *103*, 9482–9487.

(18) Dieterich, D. C.; Lee, J. J.; Link, A. J.; Graumann, J.; Tirrell, D. A.; Schuman, E. M. *Nat. Protoc.* **2007**, *2*, 532–540.

(19) Bagert, J. D.; Xie, Y. J.; Sweredoski, M. J.; Qi, Y.; Hess, S.; Schuman, E. M.; Tirrell, D. A. *Mol. Cell Proteomics* **2014**, *13*, 1352–1358.

(20) Howden, A. J. M.; Geoghegan, V.; Katsch, K.; Efstathiou, G.; Bhushan, B.; Boutureira, O.; Thomas, B.; Trudgian, D. C.; Kessler, B. M.; Dieterich, D. C.; Davis, B. G.; Acuto, O. *Nat. Methods* **2013**, *10*, 343–346.

(21) Bagert, J. D.; van Kessel, J. C.; Sweredoski, M. J.; Feng, L.; Hess, S.; Bassler, B. L.; Tirrell, D. A. *Chem. Sci.* **2016**, *7*, 1797–1806.

(22) Feng, L.; Rutherford, S. T.; Papenfort, K.; Bagert, J. D.; van Kessel, J. C.; Tirrell, D. A.; Wingreen, N. S.; Bassler, B. L. *Cell* **2015**, *160*, 228–240.

(23) Kramer, G.; Sprenger, R. R.; Back, J.; Dekker, H. L.; Nessen, M. A.; van Maarseveen, J. H.; de Koning, L. J.; Hellingwerf, K. J.; de Jong, L.; de Koster, C. G. *Mol. Cell Proteomics* **2009**, *8*, 1599–1611.

(24) Sinai, L.; Rosenberg, A.; Smith, Y.; Segev, E.; Ben-Yehuda, S. *Mol. Cell* **2015**, *57*, 695–707.

(25) Tanrikulu, I. C.; Schmitt, E.; Mechulam, Y.; Goddard, W. A.; Tirrell, D. A. *Proc. Natl. Acad. Sci. U.S.A.* **2009**, *106*, 15285–15290.

(26) Grammel, M.; Zhang, M. M.; Hang, H. C. *Angew. Chem. Int. Ed.* **2010**, *49*, 5970–5974.

(27) Grammel, M.; Dossa, P. D.; Taylor-Salmon, E.; Hang, H. C. *Chem. Commun.* **2012**, *48*, 1473–1474.

(28) Ngo, J. T.; Champion, J. A.; Mahdavi, A.; Tanrikulu, I. C.; Beatty, K. E.; Connor, R. E.; Yoo, T. H.; Dieterich, D. C.; Schuman, E. M.; Tirrell, D. A. *Nat. Chem. Biol.* **2009**, *5*, 715–717.

(29) Ngo, J. T.; Babin, B. M.; Champion, J. A.; Schuman, E. M.; Tirrell, D. A. *ACS Chem. Biol.* **2012**, *7*, 1326–1330.

(30) Xu, K. D.; Franklin, M. J.; Park, C. H.; McFeters, G. A.; Stewart, P. S. *FEMS Microbiol. Lett.* **2001**, *199*, 67–71.

(31) Amann, E.; Ochs, B.; Abel, K. J. *Gene* **1988**, *69*, 301–315.

(32) Winsor, G. L.; Lam, D. K. W.; Fleming, L.; Lo, R.; Whiteside, M. D.; Yu, N. Y.; Hancock, R. E. W.; Brinkman, F. S. L. *Nucleic Acids Res.* **2011**, *39*, D596–D600.

(33) Zimmermann, A.; Reimmann, C.; Galimand, M.; Haas, D. *Mol. Microbiol.* **1991**, *5*, 1483–1490.

(34) Latifi, A.; Foglino, M.; Tanaka, K.; Williams, P.; Lazdunski, A. *Mol. Microbiol.* **1996**, *21*, 1137–1146.

(35) Dasgupta, N.; Wolfgang, M. C.; Goodman, A. L.; Arora, S. K.; Jyot, J.; Lory, S.; Ramphal, R. *Mol. Microbiol.* **2003**, *50*, 809–824.

(36) Suh, S.-J.; Runyen-Janecky, L. J.; Maleniak, T. C.; Hager, P.; MacGregor, C. H.; Zielinski-Mozny, N. A.; Phibbs, P. V.; West, S. E. H. *Microbiology* **2002**, *148*, 1561–1569.

(37) Lee, S.; Hinz, A.; Bauerle, E.; Angermeyer, A.; Juhaszova, K.; Kaneko, Y.; Singh, P. K.; Manoil, C. *Proc. Natl. Acad. Sci. U.S.A.* **2009**, *106*, 14570–14575.

(38) Werner, E.; Roe, F.; Bugnicourt, A.; Franklin, M. J.; Heydorn, A.; Molin, S.; Pitts, B.; Stewart, P. S. *Appl. Environ. Microb.* **2004**, *70*, 6188–6196.

(39) Cavallari, J. F.; Lamers, R. P.; Scheurwater, E. M.; Matos, A. L.; Burrows, L. L. *Antimicrob. Agents Ch.* **2013**, *57*, 3078–3084.

(40) Nair, S.; Finkel, S. E. *J. Bacteriol.* **2004**, *186*, 4192–4198.

(41) Calhoun, L. N.; Kwon, Y. M. *J. Appl. Microbiol.* **2011**, *110*, 375–386.

(42) Almirón, M.; Link, A. J.; Furlong, D.; Kolter, R. *Genes Dev.* **1992**, *6*, 2646–2654.

(43) Ramsey, D. M.; Wozniak, D. J. *Mol. Microbiol.* **2005**, *56*, 309–322.

(44) Stapper, A. P.; Narasimhan, G.; Ohman, D. E.; Barakat, J.; Hentzer, M.; Molin, S.; Kharazmi, A.; Høiby, N.; Mathee, K. *J. Med. Microbiol.* **2004**, *53*, 679–690.

(45) Battesti, A.; Majdalani, N.; Gottesman, S. *Annu. Rev. Microbiol.* **2011**, *65*, 189–213.

(46) Oliver, J. D. *FEMS Microbiol. Rev.* **2010**, *34*, 415–425.

(47) Ayrapetyan, M.; Williams, T. C.; Oliver, J. D. *Trends Microbiol.* **2015**, *23*, 7–13.

(48) Brazas, M. D.; Hancock, R. E. W. *Antimicrob. Agents Ch.* **2005**, *49*, 3222–3227.

(49) Linares, J. F.; Gustafsson, I.; Baquero, F.; Martinez, J. L. *Proc. Natl. Acad. Sci. U.S.A.* **2006**, *103*, 19484–19489.

(50) Schlacher, K.; Goodman, M. F. *Nat. Rev. Mol. Cell Biol.* **2007**, *8*, 587–594.

(51) Barken, K. B.; Pamp, S. J.; Yang, L.; Gjermansen, M.; Bertrand, J. J.; Klausen, M.; Givskov, M.; Whitchurch, C. B.; Engel, J. N.; Tolker-Nielsen, T. *Environ. Microbiol.* **2008**, *10*, 2331–2343.

(52) Van Acker, H.; Sass, A.; Bazzini, S.; De Roy, K.; Udine, C.; Messiaen, T.; Riccardi, G.; Boon, N.; Nelis, H. J.; Mahenthiralingam, E.; Coenye, T. *PLoS ONE* **2013**, *8*, e58943.

(53) McKinney, J. D.; Höner zu Bentrup, K.; Muñoz-Elías, E. J.; Miczak, A.; Chen, B.; Chan, W. T.; Swenson, D.; Sacchettini, J. C.; Jacobs, W. R.; Russell, D. G. *Nature* **2000**, *406*, 735–738.

(54) Kohanski, M. A.; Dwyer, D. J.; Hayete, B.; Lawrence, C. A.; Collins, J. J. *Cell* **2007**, *130*, 797–810.

(55) Nandakumar, M.; Nathan, C.; Rhee, K. Y. *Nat. Commun.* **2014**, *5*, 4306.

(56) Muñoz-Elías, E. J.; Upton, A. M.; Cherian, J.; McKinney, J. D. *Mol. Microbiol.* **2006**, *60*, 1109–1122.

(57) Brock, M.; Maerker, C.; Schütz, A.; Völker, U.; Buckel, W. *EMBO J. Biochem.* **2002**, *269*, 6184–6194.

(58) Choi, K.-H.; Schweizer, H. P. *Nat. Protoc.* **2006**, *1*, 153–161.

(59) Koch, B.; Jensen, L. E.; Nybroe, O. *J. Microbiol. Meth.* **2001**, *45*, 187–195.

(60) Guzman, L. M.; Belin, D.; Carson, M. J.; Beckwith, J. *J. Bacteriol.* **1995**, *177*, 4121–4130.

(61) West, S. E.; Schweizer, H. P.; Dall, C.; Sample, A. K.; Runyen-Janecky, L. J. *Gene* **1994**, *148*, 81–86.

(62) Schweizer, H. P. *Gene* **1991**, *97*, 109–121.

(63) Heydorn, A.; Nielsen, A. T.; Hentzer, M.; Sternberg, C.; Givskov, M.; Ersbøll, B. K.; Molin, S. *Microbiology* **2000**, *146*, 2395–2407.

(64) Tolker-Nielsen, T.; Sternberg, C. In *Pseudomonas Methods and Protocols*, Filloux, A., Ramos, J.-L., Eds.; Methods in Molecular Biology 1149, DOI: 10.1007/978-1-4939-0473-0_47; Springer New York: 2014, pp 615–629.

(65) Alhede, M.; Bjarnsholt, T.; Jensen, P. Ø.; Phipps, R. K.; Moser, C.; Christophersen, L.; Christensen, L. D.; van Gennip, M.; Parsek, M.; Høiby, N.; Rasmussen, T. B.; Givskov, M. *Microbiology* **2009**, *155*, 3500–3508.

(66) Hong, V.; Presolski, S. I.; Ma, C.; Finn, M. G. *Angew. Chem. Int. Ed.* **2009**, *121*, 10063–10067.

(67) Kalli, A.; Hess, S. *Proteomics* **2012**, *12*, 21–31.

(68) Cox, J.; Mann, M. *Nat. Biotechnol.* **2008**, *26*, 1367–1372.

(69) Cox, J.; Hein, M. Y.; Luber, C. A.; Paron, I.; Nagaraj, N.; Mann, M. *Mol. Cell Proteomics* **2014**, *13*, 2513–2526.

(70) Ritchie, M. E.; Phipson, B.; Wu, D.; Hu, Y.; Law, C. W.; Shi, W.; Smyth, G. K. *Nucleic Acids Res.* **2015**, gkv007.

(71) Benjamini, Y.; Hochberg, Y. *J. Roy. Stat. Soc. B Met.* **1995**, *57*, 289–300.

(72) Hunter, J. D. *Comput. Sci. Eng.* **2007**, *9*, 90–95.

(73) Schneider, C. A.; Rasband, W. S.; Eliceiri, K. W. *Nat. Methods* **2012**, *9*, 671–675.